Nanoscale

Accepted Manuscript

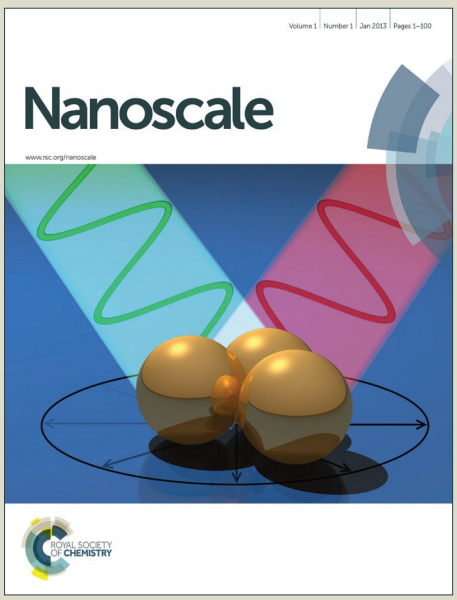

ROYAL SOCIETY OF CHEMISTRY

www.rsc.org/nanoscale

Journal Name

ARTICLE

Porous Nitrogen-doped Carbon Derived from Silk Fibroin Protein Encapsulating Sulfur as a Superior Cathode Material for High-Performance Lithium-Sulfur Batteries

Received 00th January 20xx,
Accepted 00th January 20xx

DOI: 10.1039/x0xx00000x

www.rsc.org/

Jiawei Zhang, Yurong Cai, *Qiwei Zhong, Dongzhi Lai and Juming Yao

The features of the carbon substrate are crucial for the electrochemical performance of lithium-sulfur (Li-S) batteries. Nitrogen doping of carbon materials is assumed to play an important role in sulfur immobilisation. In this study, natural silk fibroin protein is used as a precursor of nitrogen-rich carbon to fabricate a novel, porous, nitrogen-doped carbon material through facile carbonisation and activation. Porous carbon, with a reversible capacity of 815 mAh g^{-1} at 0.2 C after 60 cycles, serves as the cathode material in Li-S batteries. Porous carbon retains a reversible capacity of 567 mAh g^{-1}, which corresponds to a capacity retention of 98% at 1 C after 200 cycles. The promising electrochemical performance of porous carbon is attributed to the mesoporous structure, high specific surface area and nitrogen doping into the carbon skeleton. This study provides a general strategy to synthesise nitrogen-doped carbons with a high specific surface area, which is crucial to improve the energy density and electrochemical performance of Li-S batteries.

Introduction

With the rapidly increasing demand for electrical vehicles and portable electronic devices, rechargeable lithium-sulfur (Li-S) batteries have gained increased attention because of their high theoretical specific capacity (1672 mAh g^{-1}) and energy density (approximately 2500 Wh kg^{-1}) [1-3]. Sulfur, as one of the most abundant elements on earth, is non-poisonous, inexpensive and environment friendly. As such, sulfur is a potential electrode material for the next generation of high-performance energy storage devices [4-5]. Nevertheless, commercial application of Li-S batteries is restricted by low electrical conductivity of sulfur/polysulfides, large volume expansion of sulfur (80%) upon lithiation, dissolution of polysulfides and the resulting shuttling effect. [7, 8] Mesoporous carbon/sulfur nanocomposites have been used to resolve these limitations. The physical adsorption and high specific surface area of porous materials can inhibit the dissolution of polysulfides and allow the dispersion of the discharge products Li_2S, respectively. The high pore volume of porous materials can provide space for volume changes in sulfur, and their high conductivity can overcome electrical insulation of sulfur and its discharge products.[5, 7, 9-12]

Heterotom doping of carbon materials can induce the formation of bonds between sulfur atoms and oxygen-containing functional groups in carbon′ this process is assumed to play a key role in improving the performance of S/C cathode in lithium-sulfur batteries.[8] Guo *et al.* use boron-doped porous carbon materials as the host material of the S cathode. B atoms in carbon framework possess a partial positive charge, this polarized surface can chemically adsorb the negative polysulfides. Therefore, B dopant in S/C cathode constrains the dissolved polysulfide anions to the cathode side and enhances the cycling stability of batteries.[13] In addition, Wang *et al*. synthesised a mesoporous nitrogen-doped carbon/sulfur (MPNC/S) nanocomposite by using silica as template and poly(melamine-co-formaldehyde)resin as carbon precursor. The MPNC/S cathodes show excellent cycling stability at a high current density of 0.7 mAh cm^{-2}, with a high sulfur loading (4.2 mg S cm^{-2}) [8].

Biomass containing nitrogen has also been used to prepare N-doped carbon materials to avoid the use of chemical methods, such as sophisticated chemical procedures, in introducing nitrogen into the carbon matrix. Gelatine, chicken egg protein, eggshell membranes and prawn shells have been recently applied as efficient electrode materials in supercapacitors or Li-S battery [14-19]. For example, Shi *et al*. developed N-doped carbon by using human hair as the cheap carbon source.[20] The N-doped carbon is used as substrate to load sulfur to construct cathodes with the assistance of graphene for Li-S batteries. It was showing an improved performance of the battery due to the doping of nitrgon element and the presence of graphene. Therefore, we have reason to believe that inherent N-doped porous carbon material can improve the performances of Li-S batteries.[21]

In this study, natural silk fibroin (SF) protein, one of the main components of mulberry silk, is selected as a precursor to prepare N-doped carbon materials because of its extensive sources, low cost and high nitrogen content (approximately 16%).[22, 23] After

The Key Laboratory of Advanced Textile Materials and Manufacturing Technology of Ministry of Education, National Engineering Lab of Textile Fiber Materials & Processing Technology, College of Materials and Textiles, Zhejiang Sci-Tech University, Hangzhou 310018, China
**Corresponding author. Tel: +86 571 86843618; Fax: +86 571 86843255. E-mail:caiyr@zstu.edu.cn (Y. Cai)*

dissolution, the resulting regenerative SF solution could be manipulated to homogenously mix with the activating agent for fabricating carbon materials with abundant micropores and mesopores through carbonisation. The obtained activated silk fibroin carbon (SFC) material, which presents a high specific surface area, high electrical conductivity and abundant doping nitrogen, is then used to load sulfur by the melt diffusion technique. The electrochemical performance of the porous carbon/sulfur composite is investigated in detail. The results show that the composite can deliver a high capacity and has excellent cycling stability.

Experimental Section

Synthesis of SFC

The silk fibroin (SF) solution was prepared based on the method reported in Ref.[24, 25] Briefly, cocoons were boiled for 30 min in an aqueous solution of 0.6 wt% soap (Transfar Group Co., Ltd., Zhejiang, China), and rinsed thoroughly with water to extract the glue-like sericin proteins. The extracted silk fiber was then dissolved in an aqueous 9.3 M LiBr solution (99%; Sigma–Aldrich, St. Louis, MO, USA) at room temperature to yield a 15 wt% regenerative SF solution. This solution was dialysed in water by using the Slide-a-Lyzer dialysis cassettes (MWCO 8,000 to 13,000; Pierce, Rockford, IL, USA) for 3 d. KOH was added to a 100 mL solution of SF (5 wt%), in which the weight ratio of SF and KOH was 2:1. Finally, the SF/KOH mixture was freeze dried and carbonised at 900 °C for 2 h under a nitrogen gas (N_2) flow of 50 mL min^{-1}. The isolated particulates were washed with deionised water several times to achieve a pH of 7 and then dried in a vacuum oven at 60 °C.

Fabrication of SFC/S nanocomposite

To prepare the SFC/S nanocomposite, the mixture of SFC and element sulfur with the mass ratio of 30:70 were grinded in carbon disulfide for 0.5 h. After removing the solvent completely with volatilization, the SFC/Sulfur mixture were heated at 155 ℃ for 12 h in an Ar-filled autoclave to enable sulfur impregnation into the carbon frameworks driven by capillary force.

Material characterization

The morphology and structure of the samples were characterised through transmission electron microscope (TEM, FEI Tecani G2 F20), Field-emission scanning electron microscopy (FE-SEM, Hitachi S4800), X-ray analaysis (XRD, Rigaku RU-200BVH) and Brunauer-Emmett-Teller surface area analysis (BET, Micromeritics ASAP2020). Sulfur loading in the composite was determined by thermogravimetric analysis (TGA) in nitrogen atmosphere with a heating rate of 5 °C per min from 25 to 600 °C by using a simultaneous DSC/TGA instrument (Mettler Toledo, Columbus, OH, USA).

Electrochemical measurements

Electrochemical measurement was conducted using the 2032 foil coin cell hardware. For preparing the working electrodes, uniform slurry was prepared by mixing the active material, acetylene black and polyvinylidene difluoride at a weight ratio of 80:10:10 in NMP under vigorous stirring for 3 h. The uniform slurry was coated onto a pure aluminium foil current collector. The active material loading is about 2 mg/cm^2 for all samples in coin cells. The electrodes were vacuum dried at 80 °C for 12 h. The total material loading per electrode was approximately 2 mg cm^{-2}. Full cells were then assembled in an Ar-filled dry glove box (< 1 ppm H_2O/O_2) by using pure lithium foil as counter electrode and Celgard 2500 separators saturated with LiTFSI electrolyte. Galvanostatic charge/discharge tests were conducted using a Neware battery tester with a voltage window of 1.5-2.8 V *vs*. Li^+/Li at room temperature. Cyclic voltammetry (CV) curve measurements were conducted on a CHI660E electrochemical workstation (CH Instrument, China) at a scan rate of 0.1 mV s^{-1}. All specific capacity values were obtained based on the mass of elemental sulfur.

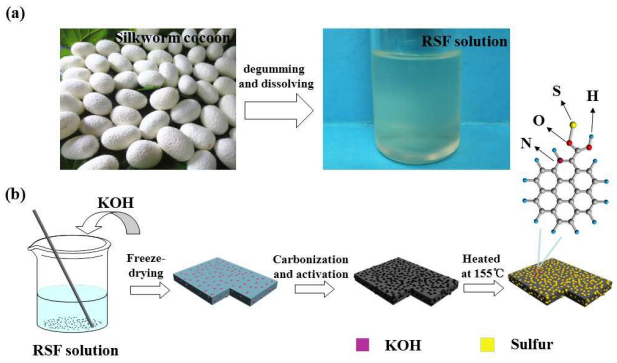

Fig. 1 Schematic illustrations of the SFC/S composites fabrication process.

Results and discussion

Generally, SF fiber could be obtained after silkworm cocoons underwent degumming. The fiber was further dissolved in aqueous LiBr solution and dialyzed in water. A high-purity regenerative SF solution was obtained (Fig. 1a). KOH, as an active agent, was added to the regenerative SF solution which was freeze dried to obtain the SF/KOH mixture. The mixture was treated at a high temperature to obtain mesoporous and N-doped carbon.[26] Finally, sulfur was incorporated into carbon through the classic melt diffusion approach. The procedure for preparing carbon/sulfur (SFC/S) nanocomposites and the proposed formation mechanism are schematically illustrated in Fig. 1b. When nitrogen is doped into the carbon matrix, the nitrogen is electron deficient and acts as electron withdrawing atom due to the higher electronegativity of nitrogen (3.0) than carbon (2.5), causing the nearby oxygen containing groups (such as carbonyl and carboxyl groups) polarized and more easily attacked by the sulfur atom as the carbon and sulfur undergo high temperature.[8]

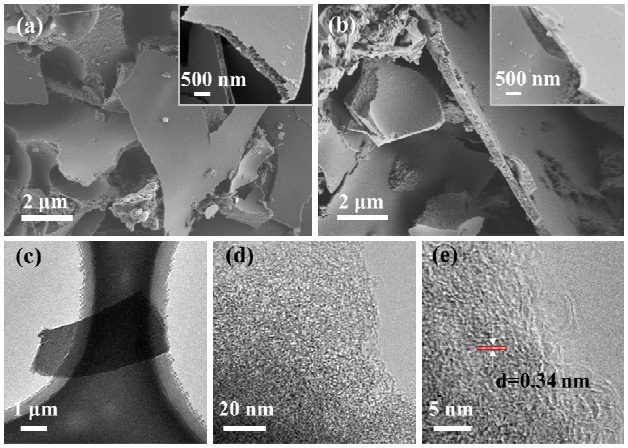

Fig. 2 FESEM images of SFC (a), SFC/S (b), and TEM images of SFC at low magnification (c), high magnification (d), and HRTEM of SFC (e).

The morphology and microstructure of the samples were investigated by FE-SEM, TEM and HR-TEM. Fig. 2a shows a typical SEM image of SFC via KOH activation. The SFC materials show lamella-like structures. In Fig. 2a inset, although the surface of SFC is smooth, its inner structure is loose and coarse, which probably due to it porous inner structure. Activated carbons are normally composed of randomly stacked graphite-like planes with a high level of disorder, which results in high porosity and specific surface area. The morphology of the SFC/S nanocomposite shown in Fig. 2b is similar to that of pure SFC. A few sulfur nanoparticles can be observed on the surface of the SFC flakes. SFC possibly exhibits high porosity, and melted sulfur completely infiltrates into SCF. Fig. 2c shows a low-magnification TEM image of SFC. The figure clearly shows that SFC present thin, lamella-like structures. Fig. 2d shows a large amount of mesopores, which lead to the high specific surface area and high porosity of SFC. The HR-TEM lattice image in Fig. 2e shows an arrangement of mostly disordered sp^2 carbon fringes for SFC. The space between two distorted lattice fringes is 0.34 nm, which is consistent with the (002) plane lattice parameter of partially graphitised SFC.[27] Therefore, we assume that the micropore structure is formed on the SFC, which is crucial for applications in Li-S batteries, considering that the composite material inhibits the dissolution of polysulfides and adapts to the volume change in sulfur.

The N_2 adsorption–desorption isotherms and pore size distribution curves of the SFC material are depicted based on the BET measurements (Figs. 3a and 3b) to validate the presence of a large amount of mesopores in SFC. The result shows that the specific surface area of the SFC material reaches 2454 $m^2\ g^{-1}$, and the total pore volume is approximately 1.5672 $cm^3\ g^{-1}$. Based on the density of sulfur (2.0 g cm^{-3}), SFC can accommodate a theoretical maximum sulfur loading of up to 76 wt%. The appropriate sulfur content of the SFC/S composite should be slightly low, considering the large volume expansion of sulfur (approximately 80%) upon lithiation. In addition, the N_2 adsorption–desorption isotherms of SFC is identified as type I isotherm with a typical microporous nature (Fig. 3a). The pore size distribution calculated by the density functional theory method indicates the prevalence of micropores and small mesopores, ranging from 1 nm to 5 nm in size (Fig. 3b). Xiao *et al*. reported that porous carbon could confine sulfur even without using any other coating; moreover, small-sized mesopores can result in higher cycling stability of the Li-S battery. Therefore, the average pore size of 2.17 nm is appropriate to inhibit polysulfide dissolution.[5] Furthermore, the large surface area and hierarchically porous structure of the carbon material contributes to confine the soluble polysulfide intermediates within the cathode and effectively alleviate the volume expansion. [14]

The XRD patterns of sulfur, SFC and SFC/S composite are shown in Fig. 3c. The broad diffraction peak of SFC at approximately 27° can be attributed to the amorphous characteristics of the carbon. The sharp diffraction peaks of pristine sulfur denote that sublimed sulfur exists in a crystalline state. For the SFC/S composite, the intensities of the sulfur characteristic peaks are weakened because of the dispersion of sulfur inside the SFC material. The thermal decomposition characteristics of pure SFC powders and SFC/S composites were further investigated using TGA to detect the loading content of sulfur in the carbon matrix. The TGA data of SFC have been provides to prove the sulfur loading (Fig. 3d). The weight loss of the SFC sample is completed at below 180 °C and the total loss weight is approximately 4%, which could be ascribed to the removal of water. The weight of SFC remains constant after 180 °C. The weight loss of the SFC/S sample occurs within the temperature range of 180 °C to 450 °C and the total loss is approximately 73%. Therefore, the weight loss of the SFC/S samples should be attributed to sulfur sublimation and we conclude that the sulfur content of SFC/S is approximately 73 wt%.

The presence of C, N, O and S atoms in SFC/S is confirmed by the result of X-ray photoelectron spectroscopy (XPS; Fig. 4a). The chemical status of S and N was further probed by analysing the high-resolution S_{2p} and N_{1s} peaks Fig. 4b shows the comparison of the XPS spectra of the SFC/S composite and pure sulfur. A peak centred at 164.1 eV is clearly observed in the spectrum of the SFC/S

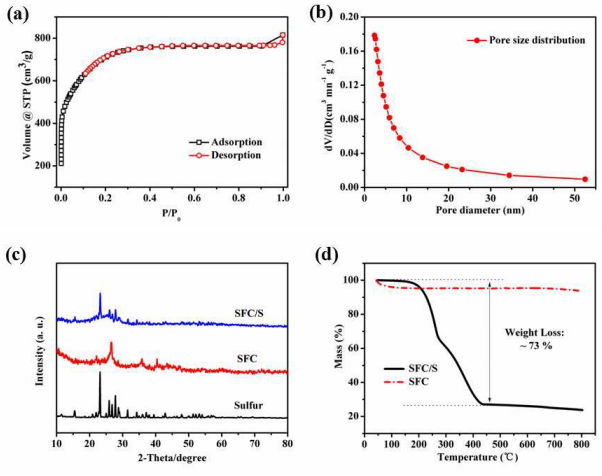

Fig. 3 Nitrogen adsorption-desorption isotherm (a), and pore size distribution curves of SFC (b), XRD patterns of Sulfur, SFC and SFC/S composites (c), TGA curve of SFC and SFC/S (d).

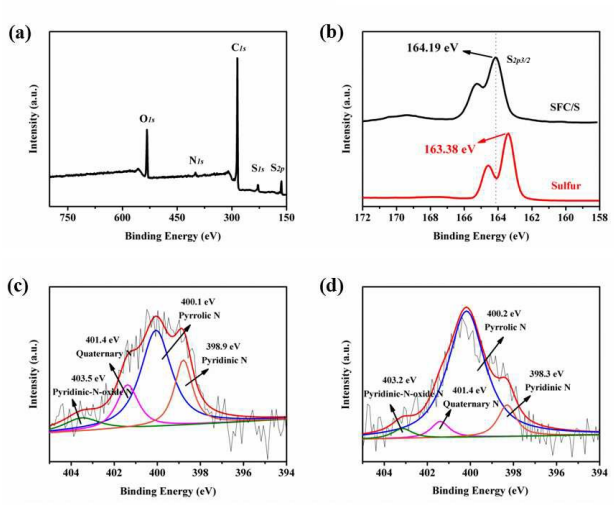

Fig. 4 XPS survey spectrum of SFC/S (a), high-resolution spectrum of the S 2p photoelectron spectra (b), and the N 1s photoelectron spectra of SFC/S (c), and SFC (d).

composite, which can be ascribed to the $2p_{3/2}$ signals of sulfur. The peaks shift to higher binding energy for 1 eV compared with their counterparts in the spectrum of pure sulfur, which can be attributed to the formation of covalent bonds directly between S and C or through the O bridge.[28, 29] Figs. 4c and 4d show the deconvoluted N_{1s} photoelectron envelopes of SFC/S and SFC. According to the XPS results, the C/N ratios of SFC and SFC/S are 25.3 and 23.8 respectively, which indicates that a larger amount of nitrogen elements are doped into the carbon. The resolved N_{1s} spectra show four different peaks revealing the presence of pyridinic N1 (398.3 ± 0.2 eV), pyrrolic N2 (400.2 ± 0.2 eV), quaternary or graphitic N3 (401.4 ± 0.2 eV) atomsnd pyridine-N-oxide N4 (403.20 ± 0.2 eV).[19] Based on the XPS results, the majority of N atoms are evidently associated in the formation of surface groups, such as pyrrolic and pyridinic nitrogen, and the other N atoms are incorporated into the carbon framework as one of its members. As previously reported,[20, 30] pyridinic and pyrrolic nitrogen exhibit the most stable configurations of adsorbing sulfur species for effectively enhancing the electrochemical performance of sulfur cathodes. Therefore, the inherent doping of nitrogen atoms in carbon-derived SF can effectively induce the chemical adsorption of sulfur on the high-surface-area carbon framework and the formation of bonds between sulfur atoms and oxygen-containing functional groups; nitrogen doping is considered important for subsequent sulfur immobilisation during the charge/discharge cycles.

Coin cells with a metallic Li counter electrode were used to evaluate the electrochemical performance of SFC/S. Fig. 5a shows the first, second and third discharge/charge profiles of the SFC/S electrode at 0.2 C (where 1 C corresponds to a current density of 1,675 mA g^{-1}) between 1.5 and 2.8 V. Two plateaus at 2.38 and 2.10 V are clearly observed during the discharge process, which correspond to the reduction of sulphur to high-order polysulphides (Li_2S_x, $4 \le x \le 8$) and low-order polysulphides (such as Li_2S_2 and Li_2S), respectively.[1, 31] During the first charge process, the long oxidation plateau from 2.20 V to 2.42 V is the reverse reaction, which corresponds to the formation of Li_2S_n ($n > 2$) and the final oxidation to S_8.[2, 32, 33] The first discharge and charge curves deliver specific capacities of 1,140 and 1,135 mAh g^{-1}, which correspond to a columbic efficiency of 100%. With continuous cycling, the electrodes exhibit typical initial capacity fading of Li–S batteries. Fig. 5b shows the cycling performance of the SFC/S electrode at a low current density of 0.2 C. Notably, the SFC/S electrode exhibits an excellent cycling stability and a high discharge capacity of 815 mAh g^{-1} after 60 cycles. The discharge/charge columbic efficiency is maintained at approximately 98% during these cycles. Based on the overall mass of SFC/S, the composite delivers a high capacity of 597 mAh g^{-1} after 60 cycles, which is higher than those of the highly ordered mesoporous carbon and hierarchically porous carbon.[27, 34]

The rate capability of SFC/S was further investigated. Fig. 5c shows the discharge/charge curves at different current densities from 0.1 C to 2 C. These profiles present similar shapes to those with low overpotentials observed at different rates. Even at high rates, the curves exhibit the typical reaction plateaus and deliver high capacities. Fig. 5d shows the excellent rate performance of the SFC/S electrode. The reversible capacities of SFC/S are 875, 730, 609 and 477 mAh g^{-1}, which correspond to 0.2, 0.5, 1 and 2 C, respectively. Notably, a reversible capacity of 896 mAh g^{-1} is recovered from the sample when the current is switched back to 0.1 C and the columbic efficiency is maintained at approximately 100%. This finding indicates the good stability of the SFC/S electrode during various rates. The long-term cycling stability of the SFC/S electrode was also tested at a high rate of 1 C after being

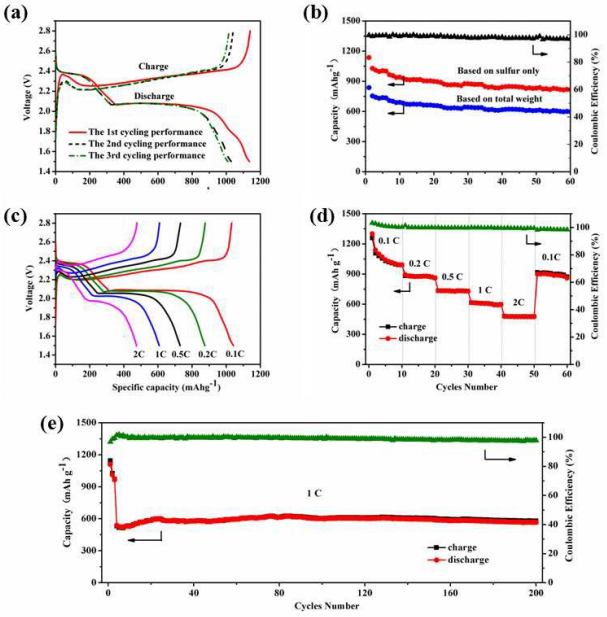

Fig.5 Electrochemical properties of the SFC/S electrode. The 1st, 2nd and 3rd discharge/charge curves (a), and cycling performance of SFC/S at 0.2 C (b). Discharge/charge profiles (c), and rate performance of SFC/S at various current densities from 0.1 C to 2 C (d). Long-term cycling performance of SFC/S electrode at a high rate of 2 C (d).

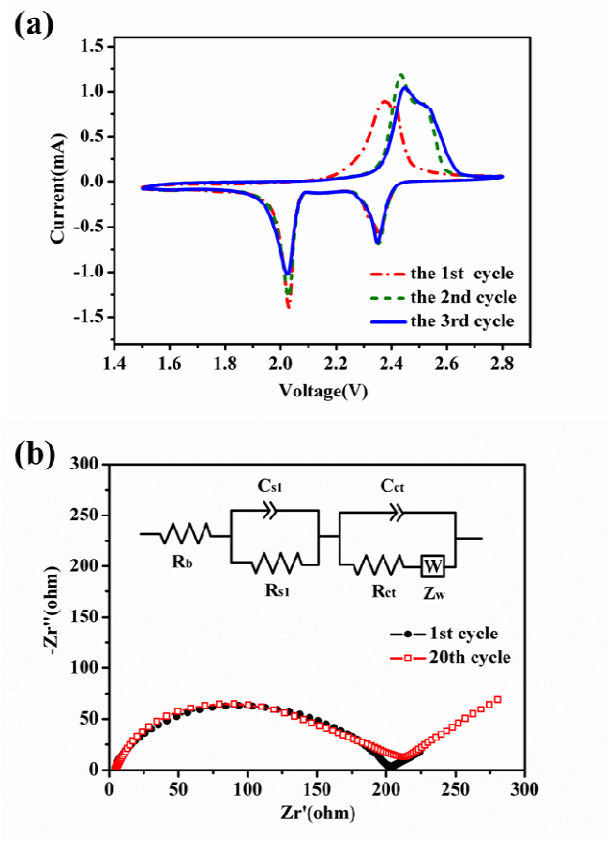

Fig. 6 Cyclic voltammetry of the initial three cycles at a scan rate of 0.1 mv/s (a), electrochemical impedance spectroscopy of the 1st and 20th cycles, the inset shows the equivalent electrical circuit model for the impedance analysis (b).

activated at 0.2 C in the initial three cycles. As shown in Fig. 5e, the current increases from 0.2 C to 1 C at the fourth cycle and the capacity of SFC/S is 539 mAh g^{-1}. In the subsequent cycle, the specific capacities tend to increase and reach the maximum value of 623 mAh g^{-1} in the 80th cycle. In addition, SFC/S maintains a capacity as high as 567 mAh g^{-1} after 200 cycles, and the columbic efficiency of the sample is maintained at approximately 98% at all times. This trend validates the good stability and reversibility of the SFC/S electrode. Such good cycling performance can be mainly attributed to the porous carbon layers, appropriate pore sizes and nitrogen doping in the carbon matrix, which effectively inhibit the dissolution of lithium polysulphide during cycles.

The cyclic voltammograms (CVs) of the SFC/S electrode were further tested within a potential window of 1.5 V to 2.8 V (*vs*. Li/Li^+) at a scan rate of 0.1 mV s^{-1} (Fig. 6a) to analyse the redox behaviour of the cathode material. During the first cathodic reduction process, a pair of sharp reduction peaks at 2.03 and 2.36 V validate that the electrochemical reduction of sulfur substantially occurs in two stages, which correspond to the two discharge plateaus shown in Fig. 5a. As previously reported,[35, 36] the first peak at 2.36 V is attributed to a fast kinetic process, which involves the conversion of elemental sulfur (S_8) to long-chain lithium polysulfides (Li_2S_n, $4 \le n \le 8$). The second reduction peak at 2.03 V is attributed to the transformation from long-chain lithium polysulfides to Li_2S_2 and eventually to Li_2S, which is a slow kinetic process that contributes to a large proportion of the capacity and is hindered by the sluggishness of solid-state diffusion in the bulk. In the first anodic process, the oxide peak at approximately 2.36 V is associated with the formation of Li_2S_n ($n > 2$). This process consists of multi-step oxidation reactions corresponding to facile conversion into intermediate S_8^{2-} at 2.36 V.[17, 37] Compared with the first CV curves, the reduction peak at the third cycle shifts slightly towards lower voltages of 2.35 and 2.02 V (*vs*. Li/Li^+), which could be ascribed to weak polarisation of the electrode after the first cycle.[38, 39]

Table 1 - Impedance parameters derived using the equivalent circuit model for the SFC/S electrodes.

Electrodes	R_b (Ω)	R_{s1} (Ω)	R_{ct} (Ω)	Z_w
SFC/S(1st cycle)	4.86	46.71	141.20	0.099
SFC/S(20th cycle)	4.50	36.18	148.50	0.026

Electrochemical impedance spectroscopy (EIS) measurements were performed to explain the interfacial charge transfer and lithium-ion diffusion processes in the SFC/S nanocomposite. As shown in Fig. 6b, the EIS spectra of the SFC/S electrode at the first and 20th cycles exhibit Nyquist plots, which consist of a depressed semicircle in the high-frequency region and an oblique line in the medium-frequency region. The diameter of the semicircle on the *Zr'*-axis is related to the interface charge transfer process of the SFC/S cathode induced by the formation of an insulating layer of lithium sulfide (Li_2S).[10, 40, 41] As shown in Table 1, the charge transfer resistances (R_{ct}) simulated from the equivalent circuits are 141.20 and 148.50 Ω after the first and 20th cycles, respectively, which indicate that the charge transfer resistance of the cathode moderately changes because of the irreversible deposition and aggregation of insoluble reduction products (Li_2S_2 and Li_2S) on the SFC/S surface during long cycling. In addition, Z_w represents the Warburg impedance, which is related to the lithium diffusion process.[10] Z_w is 0.099 for the first cycle and decreases slightly to 0.026 after the 20th cycle. Therefore, the transportation of Li^+ becomes easier as the cycle number increases, which benefits the high rate capability of the cathode during long cycling.

Conclusions

In summary, we have developed a novel, porous, nitrogen doped carbon material via a facile activation and carbonization procedure by using natural silk fibroin protein as a precursor. The obtained carbon material possesses a high special surface area of up to 2454 $m^2 g^{-1}$ and richful nitrogen element in the carbon framework. The porous N-doped carbon served as sulfur carrier in Li-S batteries and exhibited outstanding electrochemical performance,which could be ascribed to the unique architecture of material with good electrical conductivity, large special surface area and nitrogen doped. The reversible capacity of the battery could up tp 815 mAh g^{-1} at 0.2 C after 60 cycles and 567 mAh g^{-1} after 200 cycles at 1 C. We believe that these works provide novel methodology for improve the

electrochemical performance of Li-S batteries.

Acknowledgements

The work is financially supported by the Program for National Natural Science Foundation of China (51202219), Zhejiang Top Priority Discipline of Textile Science and Engineering of Open Foundation (2014KF07) and Young Researchers Foundation (2014YXQN02).

Notes and references

1 Y. Zhao, W. Wu, J. Li, Z. Xu and L. Guan, *Adv. Mater.*, 2014, **26**, 5113-5118.
2 B. Campbell, J. Bell, H. H. Bay, Z. Favors, R. Ionescu, C. S. Ozkan and M. Ozkan, *Nanoscale*, 2015, **7**, 7051-7055.
3 S. Xin, L. Gu, N. Zhao, Y. Yin, L. Zhou, Y. Guo and L. Wan, *J. Am. Chem. Soc.*, 2012, **134**, 18510-18513.
4 W. Hu, H. Zhang, Y. Zhang, M. Wang, C. Qu and J. Yi, *Chem. Commun.*, 2015, **51**, 1085-1088.
5 W. Zhou, C. Wang, Q. Zhang, H. D. Abruña, Y. He, J. Wang, S. X. Mao and X. Xiao, *Adv. Energy Mater.*, 2015, **4**, 1752-1761.
6 Y. Fu, C. Zu and A. Manthiram, *J. Am. Chem. Soc.*, 2013, **135**, 18044-18047.
7 M. Wang, W. Wang, A. Wang, K. Yuan, L. Miao, X. Zhang, Y. Huang, Y. Zhongbao and Q. Jingyi, *Chem. Commun.*, 2013, **49,** 10263-10265.
8 J. Song, T. Xu, M. L. Gordin, P. Zhu, D. Lv, Y. Jiang, Y. Chen, Y. Duan and D. Wang, *Adv. Funct. Mater.*, 2014, **24**, 1243-1250 .
9 K. H. Kim, Y. Jun, J. A. Gerbec, K. A. See, G. D. Stucky and H. Jung, *Carbon*, 2014, **69**, 543-551.
10 B. Ding, C. Yuan, L. Shen, G. Xu, P. Nie and X. Zhang, *Chem-Eur. J.*, 2013, **19**, 1013-1019.
11 X. Ji, S. Evers, R. Black and L. F. Nazar, *Nat. Commun.*, 2011, **2**, 325.
12 X. Ji, K. T. Lee and L. F. Nazar, *Nat. Mater.*, 2009, **8**, 500-506.
13 C. Yang, Y. Yin, H. Ye, K. Jiang, J. Zhang and Y. Guo, *ACS Appl. Mater. Inter.,* 2014, **6**, 8784-8795.
14 B. Zhang, M. Xiao, S. Wang, D. Han, S. Song, G. Chen, and Y. Meng, *ACS Appl. Mater. Inter.,* 2014, **6**, 13174-12182.
15 S. Chung and A. Manthiram, *Adv. Mater.*, 2014, **26**, 1360-1365.
16 X. Y. Chen, C. Chen, Z. J. Zhang, D. H. Xie and J. W. Liu, *J. Mater. Chem. A*, 2013, **1**, 4017-4025.
17 Z. Li, Z. Xu, X. Tan, H. Wang, C. M. Holt, T. Stephenson, B. C. Olsen and D. Mitlin, *Energ. Environ. Sci.*, 2013, **6**, 871-878.
18 R. J. White, M. Antonietti and M. Titirici, *J. Mater. Chem.*, 2009, **19**, 8645-8650.
19 J. Wu, C. Chen, Y. Hao and C. Wang, *Colloid. Surface. A,* 2015, **468**, 17-21.
20 M. Yu, R. Li, Y. Tong, Y. Li, C. Li, J. Hong and G. Shi, *J. Mater. Chem. A*, 2015, **3**, 9609-9615.
21 Y. Mao, H. Duan, B. Xu, L. Zhang, Y. Hu, C. Zhao, Z. Wang, L. Chen and Y. Yang, *Energ. Environ. Sci.*, 2012, **5**, 7950-7955.
22 V. Sahu, S. Grover, B. Tulachan, M. Sharma, G. Srivastava, M. Roy, M. Saxena, N. Sethy, K. Bhargava and D. Philip, *Electrochim Acta*, 2015, **160**, 244-253.
23 J. Hou, C. Cao, F. Idrees and X. Ma, *ACS nano*, 2015, **9**, 2556-2564.
24 Y. S. Yun, S. Y. Cho, H. Kim, H. J. Jin and K. Kang, *ChemElectroChem*, 2015, **2**, 359-365.
25 A. S. Lammel, X. Hu, S. H. Park, D. L. Kaplan and T. R. Scheibel, *Biomaterials*, 2010, **31**, 4583-4591.
26 Y. Zhu, S. Murali, M. D. Stoller, K. J. Ganesh, W. Cai, P. J. Ferreira, A. Pirkle, R. M. Wallace, K. A. Cychosz and M. Thommes, *Science*, 2011, **332**, 1537-1541.
27 X. Tao, X. Chen, Y. Xia, H. Huang, Y. Gan, R. Wu and F. Chen, *J. Mater. Chem. A*, 2013, **1**, 3295-3301.
28 Z. Zhang, Z. Li, F. Hao, X. Wang, Q. Li, Y. Qi, R. Fan and L. Yin, *Adv. Funct. Mater.*, 2014, **24**, 2500-2509.
29 K. Jin, X. Zhou, L. Zhang, X. Xin, G. Wang and Z. Liu, *J. Phys. Chem. C*, 2013, **117**, 21112-21119.
30 K. Han, J. Shen, S. Hao, H. Ye, C. Wolverton, M. C. Kung and H. H. Kung, *ChemSusChem*, 2014, **7**, 2545-2553.
31 Z. W. Seh, W. Li, J. C. Judy, G. Zheng, Y. Yang, T. M. Matthew, P. Hsu and Y. Cui, *Nat. Commun.*, 2013, **4**, 2327-2333.
32 G. Ma, Z. Wen, J. Jin, Y. Lu, X. Wu, M. Wu and C. Chen, *J. Mater. Chem. A*, 2014, **2**, 10350-10354.
33 D. Li, F. Han, S. Wang, F. Cheng, Q. Sun and W. Li, *ACS Appl. Mater. Inter.*, 2013, **5**, 2208-2213.
34 G. Xu, B. Ding, P. Nie, L. Shen, H. Dou and X. Zhang, *ACS Appl. Mater. Inter.*, 2013, **6**, 194-199.
35 W. Zhou, Y. Yu, H. Chen, F. J. DiSalvo and H. D. Abruña, *J. Am. Chem .Soc.*, 2013, **135**, 16736-16743.
36 Y. Yin, S. Xin, Y. Guo and L. Wan, *Angew. Chem. Int. Edit.*, 2013, **52**, 2-18.
37 M. Song, Y. Zhang and E. J. Cairns, *Nano Lett.*, 2013, **13**, 5891-5899.
38 Z. Wang,S. Zhang, L. Zhang, R. Lin,,X. Wu, H. Fang and Y. Ren, *J. Power Sources*, 2014, **248**, 337-342.
39 J. Huang, T. Zhuang, Q. Zhang, H. Peng, C. Chen and F. Wei, *ACS Nano*, 2015, **9**, 3002-3011.
40 K. H. Kim, Y. Jun, J. A. Gerbec, K. A. See, G. D. Stucky and H. Jung, *Carbon*, 2014, **69**, 543-551.
41 S. Chen, X. Huang, H. Liu, B. Sun, W. Yeoh, K. Li, J. Zhang and G. Wang, *Adv. Energy Mater.*, 2014, **4**, 1761-1770.